Compressive Sensing Taylor-Fourier Multifrequency Approach for Three-Phase Signals

Guglielmo Frigo
Lab. of Electr. Energy and Power
Swiss Federal Institute of Metrology
Bern-Wabern, Switzerland
guglielmo.frigo@metas.ch

Paolo Attilio Pegoraro
Dept. of Electr. and Electron. Eng.
University of Cagliari
Cagliari, Italy
paolo.pegoraro@unica.it

Sergio Toscani
DEIB
Politecnico di Milano
Milano, Italy
sergio.toscani@polimi.it

***Abstract*—Phasor Measurement Units represent nowadays a key technology for the development of new monitoring and control applications in transmission and, in a likely future scenario, also distribution systems. For this reason, a lot of effort is ongoing in designing PMU algorithms that are more accurate and responsive. In this regard, addressing the problem of tracking faster dynamics while cancelling the impact of harmonics, interharmonics and wideband disturbances has great relevance. This paper leverages the properties of three-phase signals to unlock the potentiality of recently proposed compressive sensing weighted Taylor-Fourier multifrequency (CS-WTFM) models to design a new algorithm (CS3-WTFM) with higher performance, particularly in the presence of interharmonic interference. Simulations prove CS3-WTFM effectiveness with reductions of total vector, frequency and rate of change of frequency errors of one or even two orders of magnitude under several testing conditions.**

***Index Terms*—Phasor Measurement Unit (PMU), Compressive Sensing, Taylor-Fourier Multifrequency, Three-phase Signals, Rate Of Change Of Frequency (ROCOF)**

I. Introduction

Phasor Measurement Units (PMUs) represented a major technological breakthrough in the monitoring of transmission grids [1]. For the first time, they made available frequent snapshots of phasors, frequency and rate of change of frequency (ROCOF) in geographically remote nodes, timestamped according to a shared time coordinate. Measurement accuracy provided by PMUs strongly depends on the adopted algorithm [2]–[4]. In this respect, standard IEC 60255-118-1:2018 [5] (IEC Std in what follows) defines two performance classes (P intended for low latency and fast response, M for high accuracy in slowly-varying conditions) as well as the requirements that the algorithm shall fulfil under different scenarios.

Dr Frigo's work was supported by the SFOE QUINPORTION Research Program under Grant SI/502415.

Dr. Pegoraro's work was funded by European Union – Next Generation EU through the Italian Ministerial grant PRIN 2022 "Smart grid-connected power converters based on advanced synchrophasor-inspired harmonics measurements for holistic integration of renewable energy sources (POWERHERO)," n. 20224X2AYH, CUP F53D23000490006.

Dr. Toscani's work was funded by European Union – Next Generation EU through the Italian Ministerial grant PRIN 2022 "Next-generation distributed synchronized measurement systems for smart grids with self-diagnostics capabilities and self-improvement of information quality," n. 2022RYZJT9, CUP D53D23001470006.

A large number of PMU algorithms can be found in the scientific literature, based on multifold approaches [6]–[9]. Recently, efforts have been focused on enhancing the dynamic response, or on guaranteeing low latency and high accuracy also in the presence of interharmonics or complex disturbances, considering more challenging conditions with respect to those prescribed by compliance tests. This research is stimulated by the future installation of PMU-like devices in distribution networks [10], [11]. With respect to conventional PMUs, they face highly dynamic conditions in the presence of significant harmonics and interharmonics [12], [13].

Among all the algorithms, those based on Taylor-Fourier Filters (TFFs) [14] are particularly interesting, thanks to their flexibility. They are suitable for tracking fast dynamics, as well as providing cancellation of disturbances coming from harmonics and interharmonics that could be included in the signal model, leading to the Taylor Fourier Multifrequency (TFM) approach [15]. Considering TFM-based methods, one may assume that interference is due to a sparse set of narrowband components, which can be identified by solving a compressive sensing (CS) problem, in turn enabling adaptive suppression of interferers. Performance highly depends on a proper retrieval of such components, representing the spectral support of the signal: mistakes undermine the resulting filtering capability.

It is worth noting that power systems are inherently three-phase and *quasi*-balanced, thus meaning that the phase waveforms are very close to be identical, except for a time delay of one third of a period. This peculiar feature leads to the formulation of inherently three-phase synchrophasor measurement methods [16], [17] or to the improvement of approaches originally intended for single-phase operation [18], [19].

In the present paper, the CS-Weighted TFM (CS-WTFM) approach [20] has been revisited to effectively cope with the three phases. In particular, the enhanced spectral support recovery exploits the three-phase symmetry of the signal, contrasting with the inherently unbalanced nature of disturbances such as noise and interharmonics. Results highlight the remarkable performance improvement achieved by the proposed method, enabled by the more robust spectral support identification.

II. The Weighted Compressive Sensing Taylor-Fourier Multifrequency Approach

A. The Taylor-Fourier Multifrequency Model

The TFM method is based on the definition of a model for a vector of N_w samples of a real-valued signal $x(t)$, which can be expressed in the form

$$\begin{aligned}\mathbf{x}(t_r) &= \begin{bmatrix} x(t_r + \frac{N_w-1}{2}T_s) \\ \vdots \\ x(t_r) \\ \vdots \\ x(t_r - \frac{N_w-1}{2}T_s)) \end{bmatrix} = \bar{\mathbf{B}}\bar{\mathbf{p}}(t_r) + \mathbf{e} = \\ &= \left[\bar{\mathbf{\Phi}}_1\mathbf{A}_1 \cdots \bar{\mathbf{\Phi}}_S\mathbf{A}_S \;\; \bar{\mathbf{\Phi}}_1^{\mathsf{H}}\mathbf{A}_1 \cdots \bar{\mathbf{\Phi}}_S^{\mathsf{H}}\mathbf{A}_S\right]\bar{\mathbf{p}}(t_r) + \mathbf{e},\end{aligned} \tag{1}$$

where t_r is the measurement instant and T_s is the sampling time. Overbars indicate complex-valued quantities, while $^{\mathsf{H}}$ denotes the Hermitian operator. In the following, without loss of generality, N_w is assumed to be an odd number, so that the sample collected in $t = t_r$ corresponds to the central element of vector $\mathbf{x}(t_r)$. Vector $\mathbf{e}$ includes all model errors while $\bar{\mathbf{p}}(t_r)$ is the vector of the model parameters to be estimated, which can be written as

$$\bar{\mathbf{p}} = \left[\bar{X}_1^{(0)} \cdots \bar{X}_1^{(K_1)} \cdots \bar{X}_S^{(0)} \cdots \bar{X}_S^{(K_S)} \;\; \underline{X}_1^{(0)} \cdots \underline{X}_S^{(K_S)}\right]^{\mathsf{T}}. \tag{2}$$

$\bar{\mathbf{p}}$ includes the phasors $\bar{X}_s^{(0)}$ (with $s \in \{1, \ldots, S\}$) of all the considered components in the signal along with their successive derivatives $\bar{X}_s^{(k)}$ (with $k = 1, \ldots, K_s$, being K_s the expansion order) evaluated in $t = t_r$. Also the conjugates of these parameters (indicated through the underbar) must be included since the signal is real-valued by assumption.

According to (1), two types of matrices are used to define the model, i.e.

$$\bar{\mathbf{\Phi}}_s = \begin{bmatrix} e^{j\omega_s \frac{N_w-1}{2}T_s} & & & & \\ & \ddots & & & \\ & & 1 & & \\ & & & \ddots & \\ & & & & e^{-j\omega_s \frac{N_w-1}{2}T_s} \end{bmatrix} e^{j\omega_s t_r}, \tag{3}$$

which is the phase-rotation matrix, with ω_s being the center frequency of the sth component and

$$\mathbf{A}_s = \frac{1}{2}\begin{bmatrix} 1 & \frac{N_w-1}{2}T_s & \frac{\left(\frac{N_w-1}{2}T_s\right)^2}{2} & \cdots & \frac{\left(\frac{N_w-1}{2}T_s\right)^{K_s}}{K_s!} \\ \vdots & \vdots & \vdots & & \vdots \\ 1 & 0 & 0 & & 0 \\ \vdots & \vdots & \vdots & & \vdots \\ 1 & -\frac{N_w-1}{2}T_s & \frac{\left(-\frac{N_w-1}{2}T_s\right)^2}{2} & \cdots & \frac{\left(-\frac{N_w-1}{2}T_s\right)^{K_s}}{K_s!} \end{bmatrix}, \tag{4}$$

which is the Taylor time-lags matrix. The latter is the same for components with the same expansion order.

Considering power system signals, the first component always corresponds to the fundamental frequency ω_1, while the others can be both harmonics or interharmonics ($\omega_s = h_s\omega_1$ with h_s respectively integer or noninteger). The set $\{\omega_s\}_{s\in\{1,\ldots,S\}}$ ideally corresponds to the actual angular frequencies at $t = t_r$, but in practice these values are unknown, thus requiring their estimation. The presence of $\bar{X}_s^{(1)}$, which is the first derivative of the phasor corresponding to the sth component, allows frequency deviation from actual one to be accounted for in the model. This results in the need of finding only approximately the frequencies ($\tilde{\omega}_s = 2\pi\tilde{f}_s$) of the most relevant components (and thus the spectral support) of the signal to build (1).

Once the spectral support is computed and the model written, fundamental and harmonics/interharmonics dynamic phasors (in $\bar{\mathbf{p}}(t_r)$) can be found through a least squares model match, i.e.

$$\hat{\bar{\mathbf{p}}}(t_r) = \arg\min_{\bar{\mathbf{p}}} \left\|\bar{\mathbf{B}}\bar{\mathbf{p}} - \mathbf{x}(t_r)\right\|_2 = \arg\min_{\bar{\mathbf{p}}} \|\mathbf{r}(\bar{\mathbf{p}}, t_r)\|_2 \tag{5}$$

where $\|\cdot\|_2$ denotes the Euclidean norm, $\hat{}$ denotes an estimate, $\mathbf{r}$ is the residual vector for given parameters $\bar{\mathbf{p}}$ (mismatch between samples and their reconstruction from the model) and $\bar{\mathbf{B}}$ has element

$$\bar{\mathbf{c}}_{s,k}[i] = \frac{(\frac{N_w-1}{2} - i + 1)^k T_s^k}{k!} e^{j\tilde{\omega}_s(t_r + (\frac{N_w-1}{2} - i + 1)T_s)} \tag{6}$$

in its ith row and $[k+1+\sum_{i=1}^{s-1}(K_i+1)]$th column (and its conjugate at column index $k+1+\sum_{i=1}^{s-1}(K_i+1)+\sum_{i=1}^{S}(K_i+1)$). Computing such solution means approximating the available samples as a linear combination of vectors $\bar{\mathbf{c}}_{s,k}$.

Assuming full column rank, the Moore-Penrose inverse $\bar{\mathbf{B}}^{\dagger}$ provides the solution of the minimisation problem and we get

$$\hat{\bar{\mathbf{p}}}(t_r) = \bar{\mathbf{B}}^{\dagger}\bar{\mathbf{x}}(t_r) = \bar{\mathbf{H}}\bar{\mathbf{x}}(t_r) \tag{7}$$

where $\bar{\mathbf{H}} = (\bar{\mathbf{B}}^{\mathsf{H}}\bar{\mathbf{B}})^{-1}\bar{\mathbf{B}}^{\mathsf{H}}$. Matrix $\bar{\mathbf{H}}$ represents a bank of FIR filters. Its mth row $\bar{\mathbf{H}}_{m,*}$, with $\sum_{i=1}^{s-1}(K_i+1) < m \leq \sum_{i=1}^{s}(K_i+1)$, is the complex-valued unit sample response of the filter that is used to estimate $\bar{X}_s^{(l)}(t_r)$, i.e., the lth derivative of synchrophasor $\bar{X}_s^{(0)}(t_r)$ with $l = m - 1 - \sum_{i=1}^{s-1}(K_i+1)$.

A generalisation of the above approach, which was proposed in [20] and will be adopted in this paper, is obtained by weighing the samples since from the beginning with a window $\mathbf{w}[n]$ (we use a window centred in the measurement instant and thus the index $n = -\frac{N_w-1}{2}, \ldots, \frac{N_w-1}{2}$). This allows focusing on central samples, closer to the measurement instant, both at support identification and estimation stages, thus improving model definition and measurement accuracy simultaneously. Matrix $\bar{\mathbf{B}}$ columns become

$$\bar{\mathbf{c}}_{s,k}^{w} = \mathbf{W} \cdot \bar{\mathbf{c}}_{s,k} \tag{8}$$

where $\mathbf{W}$ is a diagonal matrix whose diagonal entries are given by $\mathbf{w}$. It leads to a new model matrix $\bar{\mathbf{B}}_w$, so that (5) becomes

$$\hat{\bar{\mathbf{p}}}(t_r) = \arg\min_{\bar{\mathbf{p}}} \left\|\bar{\mathbf{B}}_w\bar{\mathbf{p}} - \mathbf{x}_w(t_r)\right\|_2 = \arg\min_{\bar{\mathbf{p}}} \|\mathbf{r}_w(\bar{\mathbf{p}}, t_r)\|_2 \tag{9}$$

where $\mathbf{x}_w$ and $\mathbf{r}_w$ are the weighed counterparts of vectors $\mathbf{x}$ and $\mathbf{r}$, respectively.

If $s = 1$ is considered, $\widehat{\bar{X}}_1^{(k)}$ with $k \in \{0, 1, 2\}$ are needed to find synchrophasor, frequency and ROCOF as proven in [14]. All the quantities in this paper are referred to the measurement instant, thus, from here on, for the sake of simplicity, t_r will not be reported.

B. Compressive Sensing Solution

As mentioned in Section II-A, defining the TFM model (1) requires a set of S angular frequencies $\{\tilde{\omega}_s\}_{s\in\{1,\dots,S\}}$. To achieve accurate synchrophasor measurements the model should faithfully reflect actual components of the signal, thus finding $\tilde{\omega}_s \approx \omega_s$ represents the preliminary stage. In this paper, we rely on CS theory (as in [15]), i.e., we look for a set

$$\mathcal{S}_\omega = \{\tilde{\omega}_s, \quad s \in \{1, \dots, S\}, \quad S \leq S_{\text{max}}\} \tag{10}$$

among the frequencies belonging to the set

$$\mathcal{S} = \left\{ h\delta\omega, \quad h \in \Gamma = \left\{ 1, \dots, \left\lfloor \frac{\pi}{T_s \delta\omega} \right\rfloor \right\} \right\} = \delta\omega \cdot \Gamma \tag{11}$$

that represents a super-resolved frequency grid if $\delta\omega < \frac{2\pi}{N_w T_s}$. S_{max} is the assumed maximum number of components to seek and each $\tilde{\omega}_s$ is iteratively found as

$$\begin{aligned} \Gamma_{\mathcal{S}_\omega} = \Big\{ \widehat{h}_s, \quad s \in \{1, \dots, S\} \quad | \quad \widehat{h}_s \in \Gamma \\ \& \quad \widehat{h}_s = \underset{h\in\Gamma_s}{\arg\max} |\bar{\mathbf{d}}_h^{\mathsf{H}} \mathbf{r}_{w,s-1}| \Big\} \end{aligned} \tag{12}$$

where $\bar{\mathbf{d}}_h$ is a vector defined like $\mathbf{c}_{s,0}^w$ based on frequency $\tilde{\omega}_s = h\delta\omega$ and $\mathbf{r}_{w,s-1}$ is the weighed residual resulting from the previous iteration. $\bar{\mathbf{d}}_h$ is thus a sampled complex exponential signal with angular frequency from $\mathcal{S}$ weighed by $\mathbf{w}[n]$. At each iteration s the procedure is:

1) Define the set Γ_s of possible values for h (e.g., $\Gamma_1 = \Gamma$).
2) Find, according to (12), $\widehat{h}_s$ corresponding to maximum absolute inner product with the residual vector $\mathbf{r}_{w,s-1}$ from iteration $s-1$ ($\mathbf{r}_{w,0} = \mathbf{x}_w$).
3) Add $\widehat{h}_s\delta\omega$ to $\mathcal{S}_\omega$ and $\bar{\mathbf{d}}_{\widehat{h}_s}$ to matrix $\bar{\mathbf{B}}_{w,s}$ ($\bar{\mathbf{B}}_{w,0}$ is empty) as $\bar{\mathbf{c}}_{s,0}^w$. Add also $\bar{\mathbf{c}}_{s,k}^w$ with k up to K_s (assumed beforehand) and their complex conjugates. Remove $\widehat{h}_s$ from Γ_s, obtaining Γ_{s+1}.
4) Estimate $\widehat{\bar{\mathbf{p}}}$ as in (9) by using $\bar{\mathbf{B}}_{w,s}^\dagger$ and compute $\mathbf{r}_{w,s}$. Iterate the procedure starting again from step 1.

In the description above, h has been assumed greater than 0 for the sake of simplicity, but also direct current can be dealt with by recalling that it does not involve an image component.

Following the above procedure (CS-WTFM), spectral support and $\bar{\mathbf{p}}$ are iteratively estimated by expanding $\mathcal{S}_\omega$ at every iteration until either S_{max} is reached or $\|\mathbf{r}_{w,s}\|_2 \,/\, \|\mathbf{x}\|_2$ is below a given threshold θ_n, which can be defined fixing the minimum detectable level of spectral components or from the expected background noise. $\mathcal{S}_\omega$ is associated with the measurement instant and can thus change with time.

III. Three-Phase Extension of the CS-WTFM Method

The CS-WTFM algorithm finds at each sth iteration a new N_w-size vector $\bar{\mathbf{d}}_h$ to define $\bar{\mathbf{c}}_{s,0}^w$. Such vector is the "most similar" to the residual vector among those generated by the super-resolved grid (or a subset of it), meaning that it results in the largest projection. However, $\mathbf{r}_{w,s}$ does not simply belong to the subspace generated by vectors $\bar{\mathbf{d}}_h$ with $h \in \mathcal{S}$. Both model errors and disturbances affect projection.

In this paper, a new algorithm (CS3-WTFM) tailored for three-phase power signals is thus proposed to improve the estimation. Phase waveforms typically are close to be identical, except for a time shift of one third of the fundamental period. However, disturbances such as noise and interharmonics are asynchronous with respect to the fundamental, hence they affect each phase signal differently. On the other hand, a narrowband component at frequency ω_s, if any, appears on all phases with high probability.

Leveraging this condition, we propose to look at the signals of phases a, b and c all together when searching the spectral support. The proposed algorithm is summarised as **Algorithm 1**. At each iteration s, the three vectors corresponding to the weighed residuals of each phase ($\mathbf{r}_{w,a,s-1}$, $\mathbf{r}_{w,b,s-1}$ and $\mathbf{r}_{w,c,s-1}$ combined in matrix $\mathbf{R}_{w,abs,s-1}$) are projected on the candidate $\bar{\mathbf{d}}_h$, thus obtaining 3 inner-product results, arranged in a projection vector. All projection vectors are compared through their ℓ_1 norms and the largest norm vector corresponds to the selected index $\widehat{h}_s$. Indeed, this results in finding the candidate capturing the highest overall energy from the three-phase signal, thus reflecting the presence of significant components on all phases.

Once the best candidate at iteration s is selected, the estimated spectral support is augmented and matrix $\bar{\mathbf{B}}_{w,s}$ is obtained accordingly. The same model is used for each $\mathbf{x}_q$ ($q \in \{a, b, c\}$) and $\bar{\mathbf{p}}_q$ (the model parameters vector for phase q) is estimated as (the iteration index is here omitted for simplicity)

$$\widehat{\bar{\mathbf{p}}}_q = \bar{\mathbf{B}}_w^\dagger \bar{\mathbf{x}}_{w,q} \tag{13}$$

thus obtaining $\widehat{\bar{X}}_{1,q}^{(0)}$, i.e., an estimate of the fundamental synchrophasor of phase q, and the estimates of the phasor derivatives $\widehat{\bar{X}}_{1,q}^{(1)}$ and $\widehat{\bar{X}}_{1,q}^{(2)}$ that are used to compute frequency and ROCOF.

At every iteration, the model is refined and (13) provides updated estimates until the stop condition is met. This occurs, as mentioned above, when s reaches S_{max} or when the relative residual energy (that is $\|\mathbf{R}_{w,abc,s}\|_F \,/\, \|\mathbf{X}_{abc}\|_F$, with $\|\cdot\|_F$ indicating the Frobenius norm) is below the threshold θ_n. We can summarise the algorithm by saying that a joint support estimation is performed while looking simultaneously for the synchrophasor, frequency and ROCOF of each phase. Then frequency and ROCOF are obtained as an average of the three *per phase* values.

Algorithm 1: 3ph-CS-WTFM

Input: $\mathbf{x}_a$, $\mathbf{x}_b$, $\mathbf{x}_c$, θ_n
Output: $\mathcal{S}_\omega$, $\widehat{\bar{\mathbf{p}}}_q$ for $q \in \{a,b,c\}$
initialise $s=1$, $\mathcal{S}_{\omega,0}=\emptyset$, $\bar{\mathbf{B}}_{\frac{1}{2}w,0}=\emptyset$
initialise $\mathbf{X}_{abc}=[\mathbf{x}_a,\mathbf{x}_b,\mathbf{x}_c]$
initialise $\mathbf{X}_{w,abc}=[\mathbf{x}_{w,a},\mathbf{x}_{w,b},\mathbf{x}_{w,c}]=\mathbf{W}\mathbf{X}_{abc}$
initialise residuals $\mathbf{R}_{w,abc,0}=\mathbf{X}_{abc}$
compute residuals overall energy $\mathrm{E}_{abc,\mathrm{res}}=\|\mathbf{R}_{w,abc,0}\|_F$
while $\mathrm{E}_{abc,\mathrm{res}} \geq \theta_n \cdot \|\mathbf{X}_{abc}\|_F$ & $s \leq S_{\max}$ **do** - *support search*
  consider the appropriate Γ_s depending on the needs
  find the index $\hat{h}_s=\arg\max_{h\in\Gamma_s}\|\bar{\mathbf{d}}_h^{\mathsf{H}}\mathbf{R}_{w,abc,s-1}\|_1$
  update $\mathcal{S}_{\omega,s}=\mathcal{S}_{\omega,s-1}\cup\{\hat{h}_s\}$
  update $\bar{\mathbf{B}}_{\frac{1}{2}w,s}=\left[\bar{\mathbf{B}}_{\frac{1}{2}w,s-1} \quad \mathbf{W}\bar{\mathbf{\Phi}}_s\mathbf{A}_s\right]$
  update $\bar{\mathbf{B}}_{w,s}=\left[\bar{\mathbf{B}}_{w,\frac{1}{2},s} \quad \underline{\mathbf{B}}_{w,\frac{1}{2},s}\right]$
  find $\widehat{\bar{\mathbf{p}}}_q=\arg\min_{\bar{\mathbf{p}}}\|\mathbf{x}_{w,q}-\bar{\mathbf{B}}_{w,s}\bar{\mathbf{p}}\|_2$ for $q\in\{a,b,c\}$
  update $\mathbf{r}_{w,q,s}=\mathbf{x}_{w,q}-\bar{\mathbf{B}}_{w,s}\widehat{\bar{\mathbf{p}}}_{w,q}$ for $q\in\{a,b,c\}$ and $\mathbf{R}_{w,abc,s}=[\mathbf{r}_{w,a,s},\mathbf{r}_{w,b,s},\mathbf{r}_{w,c,s}]$
  update $\mathrm{E}_{abc,\mathrm{res}}=\|\mathbf{R}_{w,abc,s}\|_F$
  update $s=s+1$
end
return

IV. Tests and Results

Numerical simulations have been performed to assess the advantages of the proposed technique. The CS3-WTFM method has been implemented with sampling rate $f_s=5\,\mathrm{kHz}$, frequency grid resolution $\delta\omega=2\pi$ rad/s (thus corresponding to 1 Hz) and $N_w=399$ sample window length. Taylor expansion orders are assumed to be $K_1=2$ for the fundamental and $K_s=1$ for all the other components. The maximum cardinality $S_{\max}$ of the retrieved spectral support has been set to 6. The square root of a Chebyshev window has been used to define the weights $\mathbf{w}[n]$, as in [20].

CS3-WTFM has been compared with its direct competitor CS-WTFM sharing the same settings. Test duration has been set to 10 s and the reporting rate has been configured at 50 frames per second (fps), even if results have been obtained with the higher 100 fps rate for a better statistical significance.

Tests have been carried out under both static and dynamic conditions. Several test scenarios going beyond IEC Std prescriptions have been considered in order to stress the algorithm and explore its characteristics. They have been obtained by modifying some of the features of a default case, which are

- The fundamental, positive sequence component has frequency $f_1=50.05\,\mathrm{Hz}$, so that it does not belong to the 1 Hz frequency grid corresponding to $\mathcal{S}$ and allows better testing the algorithms' limits. In a real scenario, the rated frequency would clearly be part of the candidates thus leading to better performance.

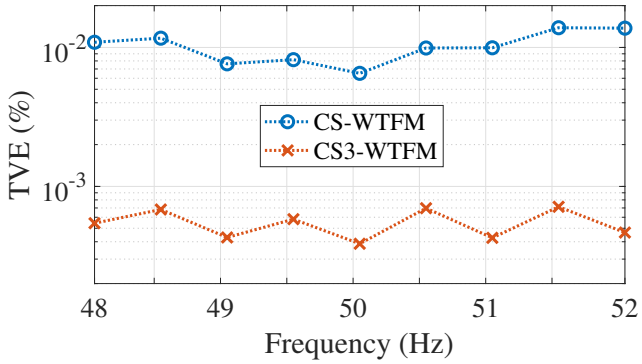

Fig. 1. Phase a maximum TVE as function of fundamental frequency for CS3-WTFM and CS-WTFM in red and blue, respectively.

- Three harmonics are always present with orders 2, 3 and 5. Their amplitudes are 3 %, 5 %, and 3 % of the fundamental, respectively, thus resulting in about 6.6 % total harmonic distortion. Three-phase symmetry is assumed (as in the harmonic distortion tests prescribed by the IEC Std [5]) hence the 2nd and 5th order harmonics are negative sequence, while the 3rd order harmonic is a zero-sequence contribution.
- A 10 % interhamonic component is included at 12.2 Hz, again not belonging to the super-resolved frequency grid. The interharmonic is positive sequence, as in the out-of-band interference test of [5].

The most significant and representative results are reported here, where performance is quantified in terms of total vector error (TVE), frequency error (FE) and ROCOF error (RFE).

Figure 1 reports the maximum TVE of phase a synchrophasor estimation when the fundamental frequency of the default case changes from 48 to 52 Hz with 0.5 Hz step. Virtually identical results can be found on the other phases, not reported here for the sake of brevity. Under off-nominal frequency conditions the TVE is rather low for both methods, but CS3-WTFM clearly outperforms CS-WTFM with errors that are more than one order of magnitude lower. It is important to underline that improvements are always due to a more accurate spectral support identification. TVE values depend on the specific frequency response of the WTFM filters, but when a harmonic or interharmonic is better modeled, a stronger cancellation of its impact in fundamental component extraction process is always possible (indeed, zeros in the FIR filter are finely tuned to eliminate the identified interference). Focusing on the sawtooth-like shape of the TVE graph for CS3-WTFM, it is interesting to notice that it is linked to the frequencies that can be included into $\mathcal{S}_\omega$: the super-resolution is 1 Hz and thus the considered fundamental frequencies are alternatively very close (0.05 Hz) or relatively far from the best grid candidate (0.45 Hz). FE and RFE also show the advantages of a better support estimation.

The above results were obtained without any wideband noise, to make more evident the differences between the two methods. However, a similar behaviour can be found when white uniform noise at different signal-to-noise ratios (SNR)

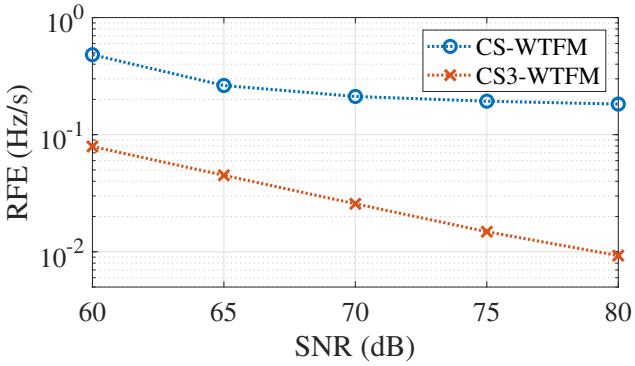

Fig. 2. Maximum RFE as function of the SNR for CS3-WTFM and CS-WTFM in red and blue, respectively.

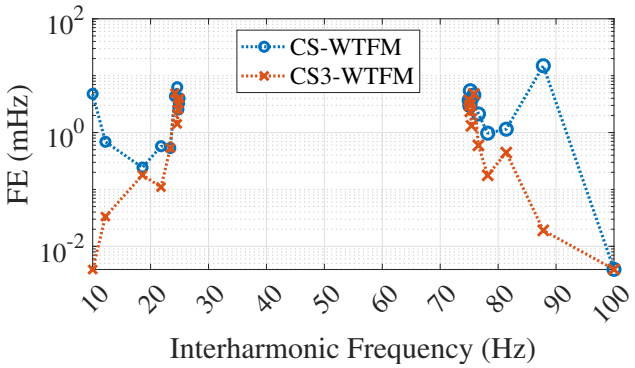

Fig. 3. Maximum FE as function of the interharmonic frequency for CS3-WTFM and CS-WTFM in red and blue, respectively.

is added to the default case. As an example, Fig. 2 depicts the RFE trend for both methods for increasing SNR. CS3-WTFM shows a linear decrease (in a log-log scale), thus highlighting the proportionality between noise standard deviation and RFE. On the other hand, considering CS-WTFM, RFE reaches a plateau when SNR exceeds 70 dB, thus revealing that, as the influence of noise declines, the other disturbances, and, in particular, that due to the interharmonic, become prevalent and their impact represents the lower bound of CS-WTFM performance. This reveals the superior rejection capabilities of CS3-WTFM, since RFE results are still dominated by noise even at 80 dB SNR.

The main advantage of the proposed CS3-WTFM approach lies in the three-phase spectral support recovery, which enables better robustness with respect to those disturbances breaking three-phase symmetry. As mentioned above, an interharmonic is inherently unbalanced, since its frequency is by definition not a multiple of the fundamental. This results in a benefit that is already evident by the previous results, but it is worth better analysing the behaviour of the algorithms by sweeping the interharmonic frequency of the default case from 10 Hz to 25 Hz, and from 75 Hz to 100 Hz, considering the values suggested by [5].

Figure 3 compares the results achieved by CS3-WTFM and CS-WTFM in terms of FE. When looking at low and high interharmonic frequency values, the advantage of the three-phase approach is remarkable. For example, considering 10 Hz interharmonic frequency, FE drops from almost 5 mHz (CS-WTFM) to $4 \cdot 10^{-3}$ mHz (CS3-WTFM). The reason for this huge difference lies in the recovered spectral support, which is ideal in the case of the three-phase method, namely the distance between the frequencies of the actual components and those recovered by the CS algorithm is below half the step of the super-resolved frequency grid. This is not true as far as the CS-WTFM method is concerned, thus estimates are much more affected by spectral interference. The same considerations apply to RFE, reduced from about 0.55 Hz/s to 1 mHz/s thanks to the three-phase support recovery.

The errors achieved by CS3-WTFM and CS-WTFM become similar as the interharmonic frequency is close to 25 Hz or 75 Hz, namely the PMU passband limits for 50 fps reporting rate. In those cases, the spectral support estimated by the CS3-WTFM method is better and more stable with respect to that recovered by the CS-WTFM technique, but it is no longer the optimal one. In particular, it may misposition the interharmonic component by one step of the super-resolved frequency grid.

For a deeper analysis of the interharmonic rejection capability, the default case has been modified by setting the interharmonic frequency to 10 Hz while sweeping its magnitude from 1 % to 10 %; Fig. 4 shows the resulting maximum FE values. The chosen interharmonic frequency lies on the super-resolved grid: therefore, the optimal support would be able to fully suppress its impact. As a further consideration, it is worth highlighting that the error trend results from two contrasting effects. On the one hand, it is easier to properly locate a larger interharmonic; on the other hand, it may produce stronger spectral interference with fundamental-related estimates. The CS3-WTFM method retrieves the optimal support in the whole amplitude range: this is the reason why FE remains constant. Under this condition, error is fully due to scalloping loss and spectral interference with harmonics, which cannot be fully suppressed since their frequencies do not belong to the aforementioned grid. Conversely, the conventional CS-WTFM method is not able to grasp the optimal support: in fact, error values increase with interharmonic amplitude, as a result of the stronger spectral interference.

The improvement introduced by the CS3-WTFM is particularly evident in the presence of interharmonic components, which break the three-phase symmetry. When considering dynamic conditions, the estimation errors may be dominated by the difficulty of properly identifying the time-varying parameters over a rather short observation interval, which exacerbates the infiltration of interharmonics.

Nevertheless, the three-phase formulation guarantees a more robust and stable support recovery also under dynamic conditions. Therefore, a performance improvement is noticeable also when modulations are added to the default case. In this regard, Table I reports the results. For this analysis, the P-class modulation conditions have been taken into account. Therefore, modulation frequency is limited to 2 Hz, while modulation depth is set to 0.1 and 0.1 rad for the AM and

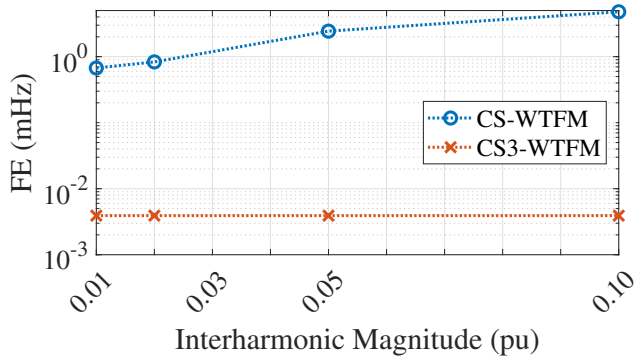

Fig. 4. Maximum FE as function of the interharmonic magnitude for CS3-WTFM and CS-WTFM in red and blue, respectively.

TABLE I
DEFAULT CASE + P-CLASS MODULATION CONDITIONS: PERFORMANCE ACHIEVED BY CS3-WTFM AND CS-WTFM

Method	TVE (%)		FE (mHz)		RFE (Hz/s)	
	AM	PM	AM	PM	AM	PM
CS3-WTFM	0.002	0.007	0.32	3.57	0.006	0.079
CS-WTFM	0.009	0.107	1.04	4.09	0.064	0.224

PM case, respectively.

It is interesting to observe how the CS3-WTFM outperforms the CS-WTFM counterpart in all the considered metrics. The improvement is particularly remarkable in the PM case, where TVE (values are identical for all the phases) is decreased by over one order of magnitude and RFE is kept below 0.1 Hz/s.

V. CONCLUSIONS

In this paper, a novel and improved version of the CS-WTFM algorithm was presented. With respect to its previous edition, the proposed CS3-WTFM technique exploits the inherent three-phase symmetry of power system signals to obtain a more accurate and robust estimate of the spectral support. This formulation allows for minimising the spurious injections of both narrow- and wide-band disturbances.

The paper presented the theoretical foundation of the CS-WTFM extension to a three-phase formulation and its performance was characterised in a significant subset of static and dynamic test conditions. The comparison against the CS-WTFM counterpart proved the improvement in terms of both estimation accuracy and rejection of spurious components. This is particularly evident in the presence of sub-harmonics, a phenomenon more and more frequent in modern power systems affected by slowly dampened oscillations.

REFERENCES

[1] J. De La Ree, V. Centeno, J. S. Thorp, and A. G. Phadke, "Synchronized phasor measurement applications in power systems," *IEEE Transactions on Smart Grid*, vol. 1, no. 1, pp. 20–27, 2010.

[2] I. Kamwa, S. R. Samantaray, and G. Joos, "Compliance analysis of pmu algorithms and devices for wide-area stabilizing control of large power systems," *IEEE Transactions on Power Systems*, vol. 28, no. 2, pp. 1766–1778, 2013.

[3] L. Piotrowski, *Application of phasor measurement units for monitoring power system dynamic performance*. CIGRE Technical Brochure, 2017.

[4] G. Frigo, A. Derviškadić, Y. Zuo, and M. Paolone, "PMU-based ROCOF measurements: Uncertainty limits and metrological significance in power system applications," *IEEE Transactions on Instrumentation and Measurement*, vol. 68, no. 10, pp. 3810–3822, 2019.

[5] IEC, "IEEE/IEC international standard - measuring relays and protection equipment - part 118-1: Synchrophasor for power systems - measurements," *IEC/IEEE 60255-118-1:2018*, pp. 1–78, 2018.

[6] A. J. Roscoe, "Exploring the relative performance of frequency-tracking and fixed-filter phasor measurement unit algorithms under c37.118 test procedures, the effects of interharmonics, and initial attempts at merging p-class response with m-class filtering," *IEEE Transactions on Instrumentation and Measurement*, vol. 62, no. 8, pp. 2140–2153, 2013.

[7] D. Belega, D. Fontanelli, and D. Petri, "Low-complexity least-squares dynamic synchrophasor estimation based on the discrete Fourier transform," *IEEE Transactions on Instrumentation and Measurement*, vol. 64, no. 12, pp. 3284–3296, 2015.

[8] V. N. Giotopoulos and G. N. Korres, "A laboratory pmu based on third-order generalized integrator phase-locked loop," *IEEE Transactions on Instrumentation and Measurement*, vol. 73, pp. 1–11, 2024.

[9] C. Huang, X. Xie, and H. Jiang, "Dynamic phasor estimation through dstkf under transient conditions," *IEEE Transactions on Instrumentation and Measurement*, vol. 66, no. 11, pp. 2929–2936, 2017.

[10] J. C. Mayo-Maldonado *et al.*, "Data-driven framework to model identification, event detection, and topology change location using d-pmus," *IEEE Transactions on Instrumentation and Measurement*, vol. 69, no. 9, pp. 6921–6933, 2020.

[11] F. Aminifar, F. Rahmatian, and M. Shahidehpour, "State-of-the-art in synchrophasor measurement technology applications in distribution networks and microgrids," *IEEE Access*, vol. 9, pp. 153 875–153 892, 2021.

[12] V. Ravindran, T. Busatto, S. K. Rönnberg, J. Meyer, and M. H. J. Bollen, "Time-varying interharmonics in different types of grid-tied pv inverter systems," *IEEE Transactions on Power Delivery*, vol. 35, no. 2, pp. 483–496, 2020.

[13] P. S. Wright, A. E. Christensen, P. N. Davis, and T. Lippert, "Multiple-site amplitude and phase measurements of harmonics for analysis of harmonic propagation on Bornholm island," *IEEE Transactions on Instrumentation and Measurement*, vol. 66, no. 6, pp. 1176–1183, 2017.

[14] J. A. de la O Serna, "Dynamic phasor estimates for power system oscillations," *IEEE Transactions on Instrumentation and Measurement*, vol. 56, no. 5, pp. 1648–1657, Oct. 2007.

[15] M. Bertocco, G. Frigo, C. Narduzzi, C. Muscas, and P. A. Pegoraro, "Compressive sensing of a Taylor-Fourier multifrequency model for synchrophasor estimation," *IEEE Transactions on Instrumentation and Measurement*, vol. 64, no. 12, pp. 3274–3283, 2015.

[16] S. Toscani, C. Muscas, and P. A. Pegoraro, "Design and performance prediction of space vector-based PMU algorithms," *IEEE Transactions on Instrumentation and Measurement*, vol. 66, no. 3, pp. 394–404, 2017.

[17] F. Messina, P. Marchi, L. Rey Vega, C. G. Galarza, and H. Laiz, "A novel modular positive-sequence synchrophasor estimation algorithm for PMUs," *IEEE Transactions on Instrumentation and Measurement*, vol. 66, no. 6, pp. 1164–1175, 2017.

[18] P. Castello, R. Ferrero, P. A. Pegoraro, and S. Toscani, "Space vector Taylor–Fourier models for synchrophasor, frequency, and ROCOF measurements in three-phase systems," *IEEE Transactions on Instrumentation and Measurement*, vol. 68, no. 5, pp. 1313–1321, 2019.

[19] R. Ferrero, P. A. Pegoraro, and S. Toscani, "Synchrophasor estimation for three-phase systems based on Taylor extended Kalman filtering," *IEEE Transactions on Instrumentation and Measurement*, vol. 69, no. 9, pp. 6723–6730, 2020.

[20] G. Frigo, P. A. Pegoraro, and S. Toscani, "Enhanced support recovery for pmu measurements based on taylor–fourier compressive sensing approach," *IEEE Transactions on Instrumentation and Measurement*, vol. 71, pp. 1–11, 2022.